Figure 2 *a* shows uplift (red colour), whereas in Figure 2 the uplift is seen in the northern part of the displacement map which is near to the epicentre of May earthquake. The subsidence is shown by blue colour in both the maps. The results are in accordance to the results reported by the European Space Agency's 'SEOM programme-InSAR ap project' team and Advanced Rapid Imaging and Analysis (ARIA) team at JPL and Caltech[7,8].

1. Mitra, S., Paul, H., Ajay Kumar, Singh, S. K., Dey, S. and Powali, D., *Curr. Sci.*, 2015, **108**(10), 1938–1943.
2. Gabriel, A. K., Goldstein, R. M. and Zebker, H. A., *J. Geophys. Res.*, 1989, **94**(B7), 9183–9191.
3. Hanssen, R. F., *Data Interpretation and Error Analysis*, Kluwer Academic, Dordrecht, 2001.
4. https://sentinel.esa.int/web/sentinel/user-guides/sentinel-1-sar (last accessed on 21 May 2015).
5. Costantini, M., *IEEE Trans. Geosci. Remote Sens.*, 1998, **36**(3), 813–821.
6. Bamler, R. and Hartl, P., *Inverse Problems*, 1998, **14**, R1–R54.
7. http://insarap.org (last accessed on 26 September 2015).
8. http://aria.jpl.nasa.gov/case_studies (last accessed on 26 September 2015).

ACKNOWLEDGEMENTS. We thank Sri Tapan Misra, Director SAC for his encouragement; P. K. Pal (Deputy Director), Dr B. S. Gohil (Group Director, ADVG EPSA, SAC, ISRO) for their constant support. We also thank European Space agency (ESA) for providing Sentinel-1 data of Nepal and the SARMAP team for providing evaluation version of SARscape 5.1.

Received 4 August 2015; revised accepted 9 October 2015

SHWETA SHARMA[1,2,*]
Y. S. RAO[2]
AJAI[1]
A. K. MATHUR[1]

[1]*Space Applications Centre (ISRO), Ahmedabad 380 058, India*
[2]*Indian Institute of Technology Bombay, Mumbai 400 076, India*
**For correspondence.*
e-mail: shweta@sac.isro.gov.in

Secondary craters detection from Mini-SAR for lunar surface age dating

Counting of crater is a widely accepted method for estimation of geologic age where there is no returned lunar sample. For lunar landing site, cratering chronology and cratering rate decay are interpreted by the empirical relationship established by plotting crater frequency versus radiometric age[1]. Surface age is determined by the observed crater size frequency distribution (CSFD) of a unit area to the production function (PF) and using the crater frequency together with a calibrated chronology function (CF). Impact craters are taken into account for dating using the crater diameter to its frequency present in an area. Impact craters result from interplanetary bombardment on the lunar surface. Lunar craters created by impact are labelled into primary and secondary craters. Primary impact craters are formed by direct meteoritic bombardment on the lunar surface. Secondary craters are formed from ejecta emitted from the primary crater. Surface age dating by CSFD technique has been used in high spatial resolution optical remote sensing datasets like the Terrain Mapping Camera (TMC)[2]. However, certain anomalies like secondary craters affecting the age determination are more readily detected in radar datasets rather than optical dataset. The ability of Mini-SAR to detect secondary craters and differentiate them from primary craters is because of the capability to utilize the polarimetric radar signatures.

Mini-SAR uses S-band (12.6 cm wavelength) to probe the far side, polar regions and particularly, the permanently shadowed region of the lunar surface. Mini-SAR contains two intensity images in *H* and *V* and two cross-power intensity images between the *H* and *V* exhibiting hybrid-polarity SAR where the transmitted field is circularly polarized, and the resulting backscatter is received in two mutually coherent linear polarizations[3]. The hybrid-polarity approach utilizes the polarized properties of the backscattered fields which are characterized as Stokes parameter[4]. The four channels of Mini-SAR were converted to Stokes parameters to generate the various daughter by-products to study the surface properties for detecting the secondary craters. The daughter by-products were noisy because of speckle; the image quality was improved by applying statistical filter followed by adaptive filters. MNF transformation was applied to the filtered images for reducing their coherent dimensionality and noise from the products. For surface dating, homogenous cratered region was selected and the diameter of the craters within the area of interest was calculated for age dating.

Radar polarimetry has the capability to better distinguish between different types of surface and subsurface physical properties than single-polarization radar imagery[5]. Capability of radar to penetrate the surface and decipher the scattering properties based on the polarization information was used for deciphering the secondary craters. The study area was conducted on the lunar north polar region with its central selenographic coordinates at 83.6 lat. and –45.2 lon. on the lunar nearside (Figure 1 *a*) near Sylvester crater.

Secondary craters were differentiated from primary craters based on their unique morphologies like high ellipticities, shallow profiles, tendency to form clusters and the occasional presence of herringbone or chevron-shape[6–8]. In the study area, however, secondary craters arrangement does not necessarily attain the morphology as mentioned. Secondary craters formed from high impact velocity lack the characteristics such as flat, shallow floor of near-field secondaries and are difficult to differentiate solely through morphology.

In radar image, the secondary craters show higher circular polarization ratio

(CPR) value with fresh and rough surfaces, which generates a contrast between the ejecta blanket and the background with low CPR. Secondary craters were distinguished based on the fact that they produce larger ejecta fragments at a given crater size than primary craters[9]. Secondary craters formed by low impact velocity ejecta often resemble primary craters when they form in isolation without clusters or chains. Such craters can be identified by the presence of central mounds[10].

Secondary craters have been detected primarily based on their shape – clustering pattern and ellipticities. However, shape alone cannot be accounted for detecting secondary craters as with the increase in distance from the impact site, the hypervelocity impact from which secondary craters are formed, becomes more similar to primary craters due to the increase in speed of the projectile. To detect this error, in the present study, CPR and SC (same sense polarization) property were used along with shape parameter. Fresh ejecta and rough surface have higher CPR value due to roughness. Also, secondary craters formed from primary impact debris have asymmetric ejecta blanket.

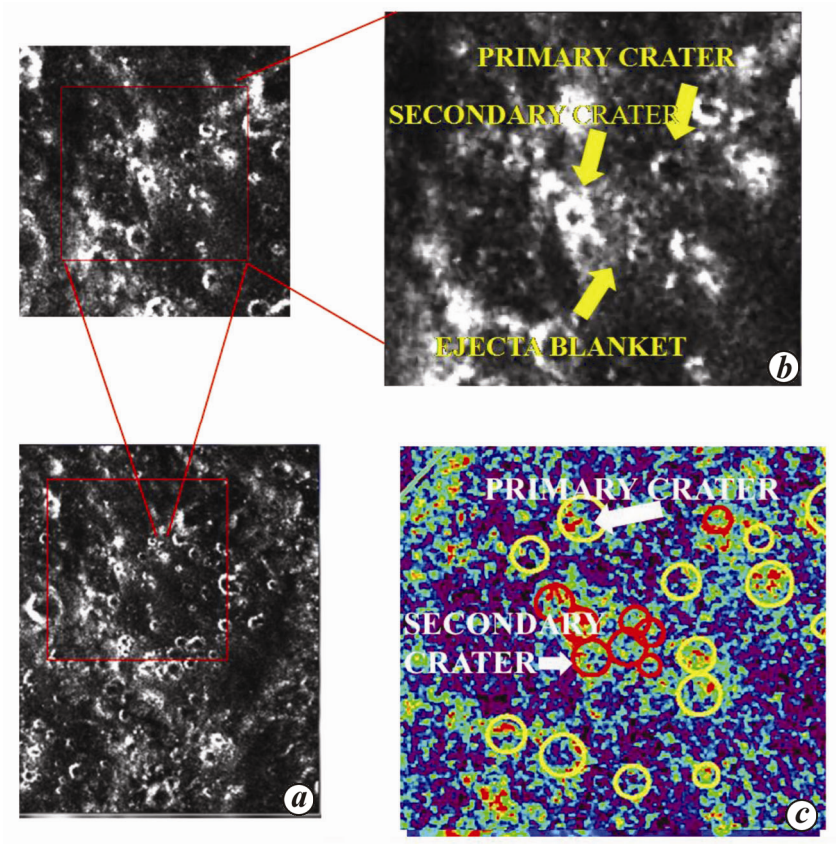

Figure 1. ***a***, Study area. ***b***, Primary and secondary craters on SC (same sense polarization) image. ***c***. Primary and secondary craters marked on circular polarization ratio image.

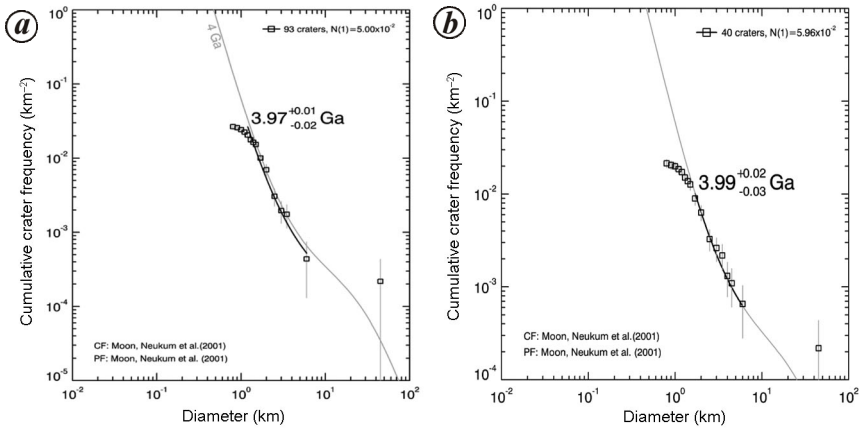

Figure 2. Lunar surface age of study area from crater size frequency distribution plot. With (***a***) and without (***b***) secondary craters.

The crater age dating of the lunar surface, especially for the polar regions was not explored much using optical sensors/images because many of these regions are permanently under shadow. Mini-SAR being an active sensor with its polarimetric property helps map and characterize the polar surfaces. Planetary surface crater dating has been studied using crater size, craters frequency, morphology distribution and relative chronology[11]. The stratigraphy of the Moon was divided into five lithostratigraphic systems corresponding to five time periods with characteristics of lunar impact. They are Pre-Nectarian (oldest), Nectarian, Imbrian, Erathosthenian and Copernican system.

Surface age dating technique is based on the concept that the observed CSFD of a given surface of known crater production function (PF) is used and the crater frequency (CF) for different crater sizes along with a calibrated CF is used to obtain absolute age[9]. The lunar production function[1] is expressed by

$$\log(N_{\text{cum}}) = a_0 + \sum_{k=1}^{11} a_k [\log(D)]^k,$$

where a_0 represents the time during which the unit has been exposed to the meteoritic bombardment. The respective cumulative crater densities of geologic units taken at a fixed reference diameter are directly related to the time in which the units were exposed to the meteorite flux and therefore represent relative age differences.

Detection of the secondary craters using the derived daughter by-products of Stokes vectors – SC and CPR parameter is shown in Figure 1 *b* and *c*. The primary crater marked on the SC image (Figure 1 *b*) is not observed in the CPR image (Figure 1 *c*) due to maturity of the crater. The crater maturity reduces

surface roughness owing to which the reflectivity of the crater is diminished leading to low backscatter. The capability of SC polarization to detect subsurface features due to diffuse scattering has been used. In SC image the primary and secondary craters (Figure 1 *b*) could be distinguished. The secondary craters clearly fall in the ejecta fragment where the signature is high due to the roughness of the fresh ejecta. Besides crater shape parameters like crater clustering pattern, elliptical shape, etc. were incorporated for identifying the secondary craters from the primary craters.

The detected secondary craters were marked and excluded from the calibration to improve the age determination of the lunar surface. The age was determined from the study area by retrieving the diameter of primary craters using three-point-based measurement system available in Cratertool software[12] and by plotting the crater counts using Craterstats software developed by Freie Universität Berlin[13]. The improved age after removing the secondary craters has been found to have better fit by the polynomial curve with lesser number of craters. With and without separating the secondary craters, the lunar surface age of the study area was found to be 3.99 and 3.97 G yr respectively (Figure 2). The derived age was compared with the USGS stratigraphic map of the Moon[14], where the study region falls under 3.20–4.53 G yr. The validation of the determined age has its limitation because of the broad stratigraphy in age group in the USGS stratigraphical map.

1. Neukum, G., Ivanov, A. and Hartmann, W. K., *Space Sci. Rev*., 2001, **96**, 55–86.
2. Arya, A. S. *et al.*, *Curr. Sci*., 2012, **102**, 783–788.
3. Spudis, P. *et al.*, *Curr. Sci*., 2009, **96**, 533–539.
4. Raney, R. K., *Geosci. Remote Sensing Lett.*, 2006, **3**(3), 317–319.
5. Carter, L. M., Campbell, D. B. and Campbell, B. A., *Proc. IEEE*, 2011, **99**(5), 770–782.
6. McEwen, A. S. *et al*., *Icarus*, 2005, **176**, 351–381.
7. Pike, R. J. and Wilhelms, D. E., Proceedings of the 9th Lunar Planet. Science Conference, Huston, Texas, 1978, pp. 907–909.
8. Oberbeck, V. R. and Morrison, R. H., In Proceedings of the Fourth Lunar Science Conference, Huston, Texas, 1973, pp. 107–123.
9. Wells, K. S., Campbell, D. B., Campbell, B. A. and Carter L. M., *J. Geophys*., 2010, **115**; doi:10.1029/2009JE00349.
10. Senthil, K. P., Kumar, A. S., Keerthi, V., Goswami, J. N., Khrishna, B. G. and Kumar, A. S. K., *Planet. Space Sci.*, 2011, **59**(9), 870–879.
11. Crater Analysis Techniques Working Group, *Icarus*, 1979, **37**, 467–474.
12. Michael, G. G. and Neukum, G., *Earth Planet. Sci. Lett.*, 2010, **294**, 223–229.
13. Kneiss, T., Gasselt, S. V. and Neukum, G., *Planet. Space Sci.*, 2010, 1243–1254.
14. Lucchitta, B. K., Geologic map of the north side of the Moon. Department of the Interior United States Geological Survey, Interior Geological Survey, Reston, 1978, VA-1978-G77061.

ACKNOWLEDGEMENTS. We thank SAC, ISRO, Ahmedabad for coordinating Chandrayaan-1 Mini-SAR Data Analysis Project under which this study was carried out.

Received 27 May 2015; revised accepted 6 October 2015

KEDOVIKHO YHOSHÜ[1,*]
R. S. CHATTERJEE[2]
P. K. CHAMPATI RAY[2]

[1]*Department of Geography,*
Nagaland University,
Headquarters Lumami,
Nagaland 798 627, India
[2]*Indian Institute of Remote Sensing,*
ISRO, 4 Kalidas Road,
Dehradun 248 001, India
**For correspondence.*
e-mail: kedovikho@gmail.com